International Journal of Biological Macromolecules 268 (2024) 131801

Contents lists available at ScienceDirect

International Journal of Biological Macromolecules

journal homepage: www.elsevier.com/locate/ijbiomac

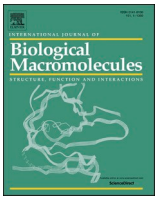

Higher-order G-quadruplex structures and porphyrin ligands: Towards a non-ambiguous relationship

Andrea Patrizia Falanga [a], Alessandro D'Urso [b], Gabriele Travagliante [b], Chiara Maria Antonietta Gangemi [b], Maria Marzano [c], Stefano D'Errico [a], Monica Terracciano [a], Francesca Greco [a], Luca De Stefano [d], Principia Dardano [d], Ilaria Rea [d], Gennaro Piccialli [a], Giorgia Oliviero [e], Nicola Borbone [a,*]

[a] Department of Pharmacy, University of Naples Federico II, via Domenico Montesano 49, 80131 Naples, Italy
[b] Department of Chemical Sciences, University of Catania, viale Andrea Doria 6, 95125 Catania, Italy
[c] CESTEV, University of Naples Federico II, via Tommaso De Amicis 95, 80145 Naples, Italy
[d] Institute of Applied Sciences and Intelligent Systems, Unit of Naples, National Research Council, via Pietro Castellino 111, 80131 Naples, Italy
[e] Department of Molecular Medicine and Medical Biotechnologies, University of Naples Federico II, via Sergio Pansini 5, 80131 Naples, Italy

ARTICLE INFO

Keywords:
G-quadruplex
Porphyrin ligands
DNA-porphyrin complexes
Polarity inversion
G-wires

ABSTRACT

Herein, we evaluated the interaction of the tetracationic porphyrin H_2TCPPSpm4 with three distinct DNA G-quadruplex (G4) models, i.e., the tetramolecular G4 d(TGGGGT)$_4$ (**Q_1**), the 5′-5′ stacked G4-dimer [d(CGGAGGT)$_4$]$_2$ (**Q_2**), and a mixture of 5′-5′ stacked G-wires [d(5′-CGGT-3′-3′-GGC-5′)$_4$]$_n$ (**Q_n**). The combined data obtained from UV–Vis, CD, fluorescence, PAGE, RLS, AFM, NMR, and HPLC-SEC experiments allowed us to shed light on the binding mode of H_2TCPPSpm4 with the three G4 models differing for the type and the number of available G4 ending faces, the length of the G4 units, and the number of stacked G4 building blocks. Specifically, we found that H_2TCPPSpm4 interacted with the shortest **Q_1** as an end-stacking ligand, whereas the groove binding mode was ascertained in the case of the **Q_2** and **Q_n** G4 models. In the case of the interaction with **Q_1** and **Q_n**, we found that H_2TCPPSpm4 induces the formation of supramolecular aggregates at porphyrin/G4 ratios higher than 2:1, whereas no significant aggregation was observed for the interaction with **Q_2** up to the 5:1 ratio. These results unambiguously demonstrated the suitability of porphyrins for the development of specific G4 ligands or G4-targeting diagnostic probes, being H_2TCPPSpm4 capable to distinguish between different G4s.

1. Introduction

G-quadruplexes (G4s) are highly ordered, non-canonical DNA structures formed by guanine-rich oligodeoxynucleotides (ODNs) [1–4]. The fundamental structural unit of a G4 is the G-tetrad, in which eight Hoogsteen hydrogen bonds hold together four guanine residues in a planar arrangement. The π–π stacking among G-tetrads leads to G4 complexes, which can be further stabilized by the presence of various cations, such as Na^+ or K^+, located in the center of the tetrad or between two of them [5]. G4s, classified in terms of stoichiometry in mono, bi, and tetramolecular based on the number of the constituting G-rich strands, exhibit high structural diversity and can form parallel, anti-parallel, or mixed hybrid structures [6,7]. G4s have interesting biological applications and can be used as anti-cancer therapeutics [8], aptamers [9,10], antiviral [11–13], and diagnostics agents [14]. However, in the last few years, G4s have also been proposed to develop tailored DNA-based supramolecular structures by a bottom-up approach. The multimerization of G4s leads to higher-ordered G4 nanostructures with significant properties through self-assembly processes [15–18]. The low cost of synthesis, the high stability in aqueous ionic solutions, the high thermal stability, the structural response to chemical stimuli, and the resistance towards DNases make G4s and related polymers one of the most versatile tools for applications in nanobiotechnology. As G4s can bind various typologies of ligands and alter their own conformational shape and stability, efforts have been devoted to synthesizing new supramolecular complexes with diverse physical-chemical behavior and new biomaterials with suitable optical, electrical, and mechanical properties [19–21]. Among G4 ligands,

* Corresponding author.
E-mail address: nicola.borbone@unina.it (N. Borbone).

https://doi.org/10.1016/j.ijbiomac.2024.131801
Received 1 November 2023; Received in revised form 29 January 2024; Accepted 17 April 2024
Available online 25 April 2024

porphyrins represent a largely studied class of DNA ligands due to their ability to interfere with primary DNA biological functions [20,22,23]. Porphyrins are planar aromatic macrocycles exhibiting peculiar electronic properties and synthetic versatility, which have been used as tools for several applications [24–27]. In addition, the size of the porphyrin core matches well that of the G-tetrad of guanines. The incorporation of cationic substituents led to porphyrin analogs with an enhanced affinity towards the DNA phosphate backbone and G4s [22,28,29]. In a previous work, we reported on the binding properties of the cationic porphyrin derivative H_2TCPPSpm4 [30], having four spermine residues linked to the *meso* positions of the tetraphenyl porphyrin core (Fig. 1), towards the G4 structure d(TGGGAG)$_4$. We observed that the porphyrin could either stack on the 5′ and 3′ faces or behave like a groove-binding ligand, thus producing stabilizing or destabilizing effects with the formation, in some cases, of G4-polymeric species [31].

In the last few years, we have studied the multimerization process that allows the obtainment of very long G4s via end-to-end π–π stacking interactions among tetramolecular monomeric G4 building blocks. In particular, the oligodeoxynucleotide (ODN) d(CGGAGGT) (**2**, Fig. 1) evolved into a stable dimeric G4 (**Q_2**, Fig. 1) through the formation of strong π–π stacking interaction between the planar octads G(:C):G(:C):G(:C):G(:C), which we named as 5′-CG sticky end, formed at the 5′ terminus of each G4 monomer (magenta circles in **Q_2**) [32,33]. To extend our studies, we developed a new kind of π–π stacked G-wire polymer (**Q_n**, Fig. 1) using the short ODN strand d(5′-CGGT-3′-3′-GGC-5′) (**3**, Fig. 1) incorporating a 3′-3′ inversion of polarity site. This short ODN formed a tetramolecular G4 building block containing two 5′-CG sticky ends and, therefore, could evolve in polymeric stacked G-wires by exploiting the 5′-5′ π–π end-stacking among several G4 units [34,35].

In this paper, we report our studies on the interaction of H_2TCPPSpm4 with the three G4 models **Q_1**, **Q_2**, and **Q_n** (Fig. 1 and Table S1 in Supplementary Data), which were chosen for their peculiar

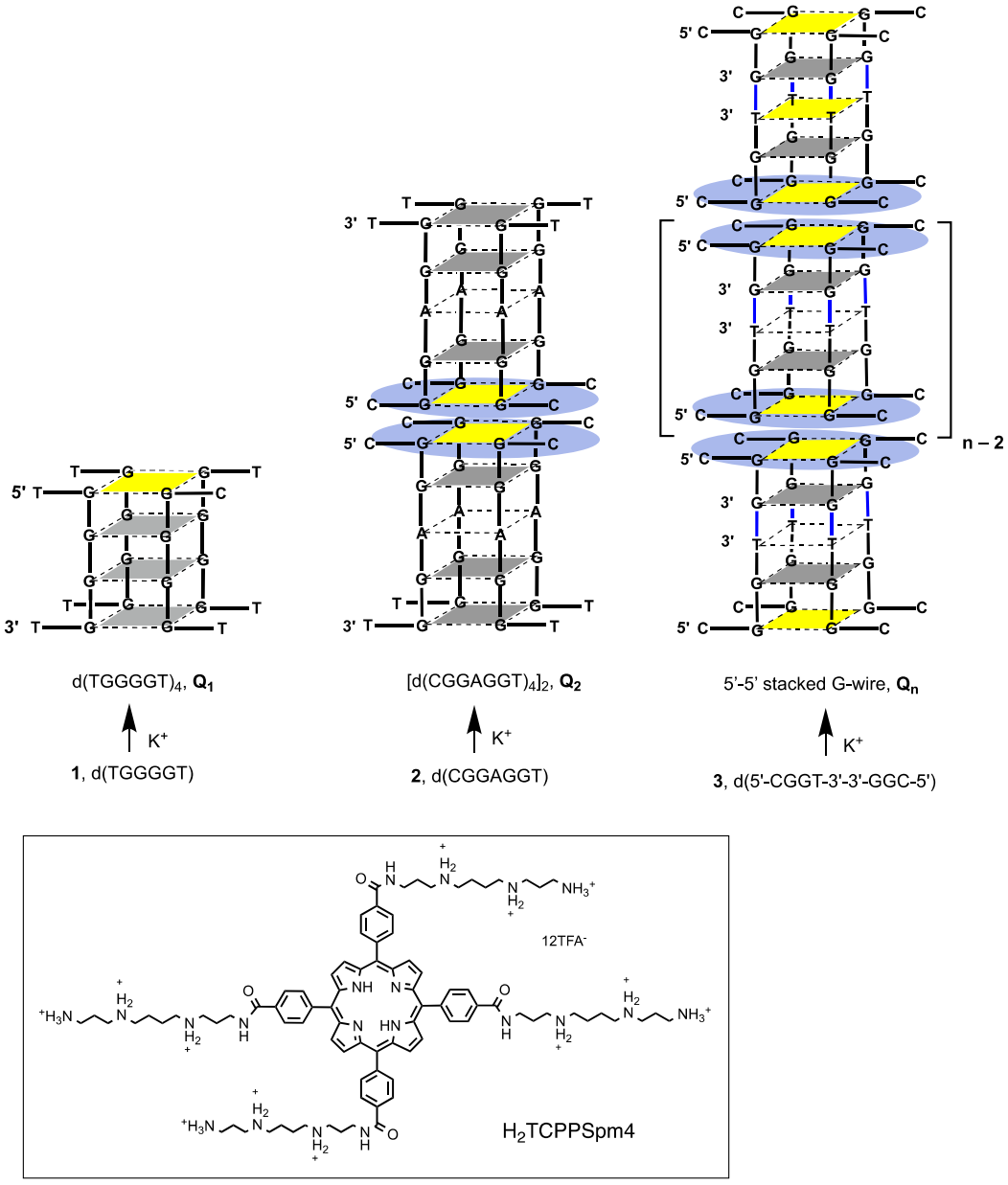

Fig. 1. Schematic representation of the G4 models **Q_1**, **Q_2**, and **Q_n**. G-tetrads are reported in gray; the G-tetrads involved in the 5′-CG sticky end are in yellow. The light blue circles indicate the planar octad G(:C):G(:C):G(:C):G(:C) system determining the 5′-CG sticky ends. The 3′-3′-phosphodiester bonds are reported in blue. The chemical structure of the tetracationic porphyrin H_2TCPPSpm4 is shown in the box. (For interpretation of the references to color in this figure legend, the reader is referred to the web version of this article.)

structural features. In detail, **Q_1** is a well-known G4 monomer model having both the 5′ and 3′ end faces available for the interaction with G4 ligands whose interaction with cationic porphyrins has been the topic of several published papers [23,36,37]; **Q_2** was chosen as a model of G4 dimer possessing only 3′-ending faces; **Q_n** was selected as a model of G-wire that differently from **Q_2** possesses only 5′-ending faces. The purpose of this investigation was twofold: firstly, deepening our understanding of the interaction between the tetracationic H_2TCPPSpm4 porphyrin and different types of parallel G4s, and, secondly, exploring the suitability of tetracationic porphyrins to obtain new G4-based composite biomaterials. Several analytical techniques, namely UV–VIS, circular dichroism (CD), polyacrylamide gel electrophoresis (PAGE), resonance light scattering (RLS), fluorescence, atomic force microscopy (AFM), size-exclusion-chromatography (HPLC-SEC), and nuclear magnetic resonance (NMR) have been used for the structural characterization of the H_2TCPPSpm4/G4 complexes.

2. Results and discussion

2.1. Preparation of the DNA G-quadruplexes Q_1, Q_2, and Q_n

The ODNs d(TGGGGT) (**1**) and d(CGGAGGT) (**2**) were synthesized using a solid-phase automated DNA synthesizer using standard phosphoramidite chemistry (Supplementary data and Materials and methods). The ODN d(5′-CGGT-3′-3′-GGC-5′) (**3**) was prepared as previously described [32]. The formation of the G4s **Q_1**, **Q_2**, and **Q_n** was obtained by dissolving the ODNs **1**–**3** respectively in 0.1 mol/L K^+-containing buffer at the single strand (SS) concentration of 6.0 mmol/L, heating them at 90 °C for 10 min and then rapidly cooling to 4 °C for 24 h. This annealing procedure allowed the formation of the G4 complexes **Q_1**, **Q_2**, and **Q_n**, whose structures were confirmed by HPLC analyses and NMR [33,35].

2.2. Interaction of H_2TCPPSpm4 with the monomeric d(TGGGGT)$_4$ G4 model (Q_1)

2.2.1. UV–VIS studies

Firstly, we performed the UV–VIS titration of **Q_1** (2 mmol/L) with

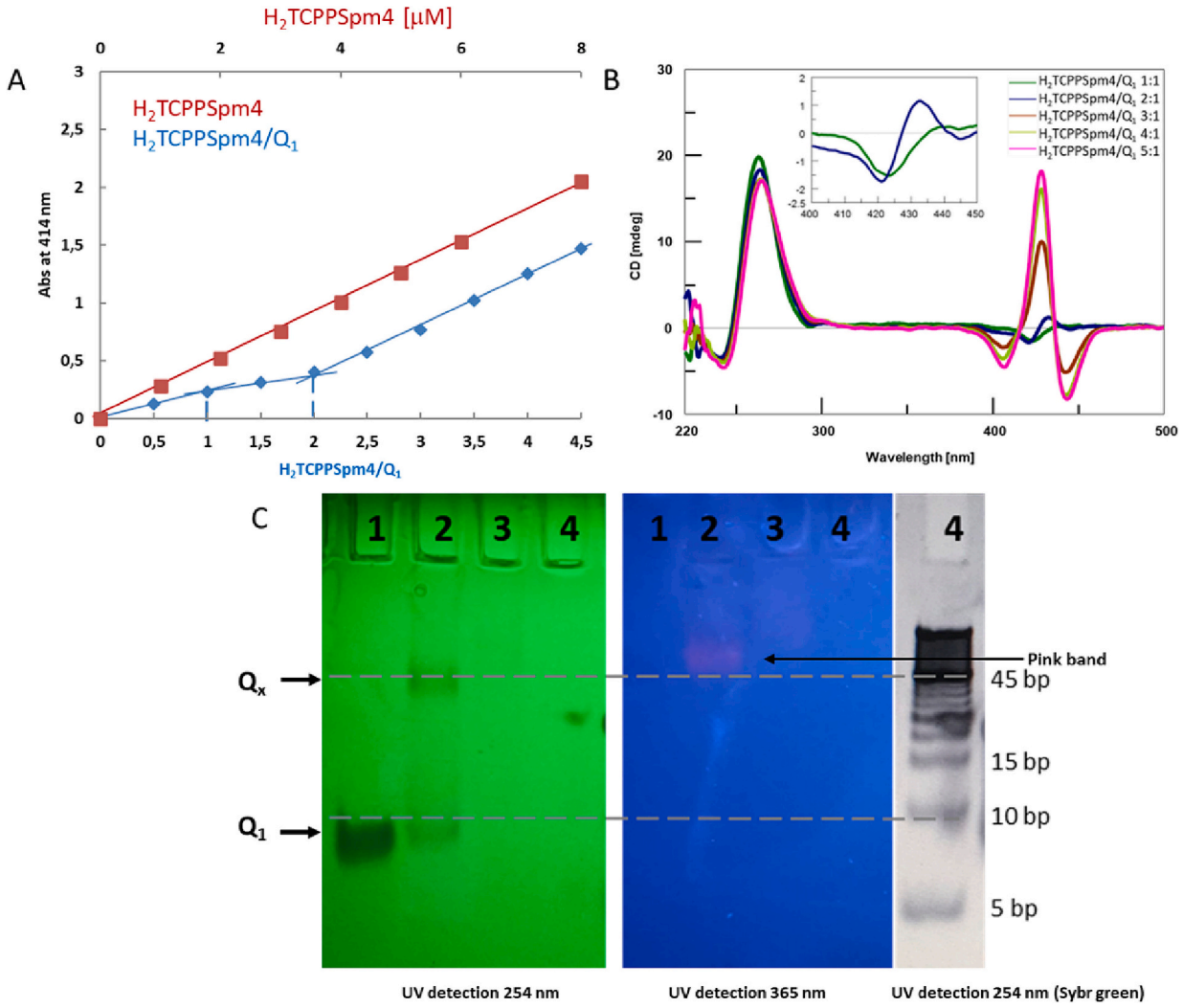

Fig. 2. (A) Soret band plot (414 nm) of increasing concentrations of H_2TCPPSpm4 alone (red line) and in the presence of the **Q_1** G4 model (blue line). (B) CD spectra of H_2TCPPSpm4/**Q_1** from 1:1 to 5:1 ratio. Inset: H_2TCPPSpm4/**Q_1** at the 1:1 and 2:1 ratio. (C) PAGE images (UV–Vis lamp 254 nm and 365 nm); the DNA ladder (lane 4) was visualized by Sybr green staining and UV transilluminator (5–100 bp). Lane 1: d(TGGGGT)$_4$ (**Q_1**); lane 2: H_2TCPPSpm4/**Q_1** at the 1:1 ratio; lane 3: H_2TCPPSpm4/**Q_1** at the 2:1 ratio. For non-processed PAGE images, refer to Fig. S18 (Supplementary data). (For interpretation of the references to color in this figure legend, the reader is referred to the web version of this article.)

increasing amounts of H_2TCPPSpm4. We report in Fig. 2A and Fig. S1 (Supplementary data) the values of the absorbance at 414 nm (Soret band, A_{414}) of the sole porphyrin, from 0 to 8.0 μmol/L concentration (red line) in comparison with the A_{414} values in the presence of **Q_1** (H_2TCPPSpm4/**Q_1** ratio, blue line) (see also Supplementary data Fig. S2A). The straight red line reveals that the porphyrin retains its monomeric aggregation state in the solution up to the concentration of 8.0 μmol/L. The UV–VIS titration of H_2TCPPSpm4 (Supplementary data Fig. S2) in the presence of 2 μmol/L of **Q_1** (blue line) showed two breakpoints at the 1:1 and 2:1 H_2TCPPSpm4/**Q_1** ratio (Fig. 2A), indicating the formation of two different species not in equilibrium with each other. After further addition of porphyrin, 3:1 ratio, we observed that the slope of the blue line became almost parallel to the red line, thus indicating no more interactions between the porphyrin and the **Q_1** G4 model. The analyses of the % of Δ slopes (Supplementary data Fig. S2B) further confirmed the presence and significance of the two breakpoints. To further discriminate the binding mode type, we calculated the hypochromic effect (ΔA_{414}) for each ratio of the H_2TCPPSpm4/**Q_1** mixture and the shift of the Soret band. In general, a slight hypochromicity (<35 %) and a slight red-shift (~8 nm) are ascribed to an external binding mode, i.e., in the grooves or by end-stacking on the 5′ or 3′ G4 face. Conversely, high shift values of the Soret band (~15 nm) and high hypochromicity (>35 %) are associated to strong π–π stacking interactions between the porphyrin and the nucleobases of G4 tetrads, as those occurring in the intercalation binding mode. As we reported in Fig. S2C (Supplementary data), at the 1:1 ratio, we observed a slight red shift (10 nm) and a low hypochromicity (29 %), which agreed with an external binding mode (in the groove or at one of the G4 ends). The increase of the H_2TCPPSpm4 concentration to the 2:1 ratio led to a significant rise in hypochromicity at 414 nm (62 %), which, however, was not coupled with an increase of the red shift of the Soret band. Taken together, the UV evidence ruled out the intercalation binding mode and supported the formation of 2:1 porphyrin/**Q_1** complexes in which the two porphyrin molecules are stacked on the top and bottom faces of the tetramolecular G-quadruplex **Q_1**, whose length allows the electronic communication between the two porphyrin chromophores which accounts for the enhanced hypochromicity. This structural hypothesis agrees well with previous reports of end-stacking interaction between cationic porphyrins and DNA G-quadruplexes [23,31,36,38–40].

2.2.2. Circular dichroism (CD) studies

The CD profile of **Q_1** in 0.1 mol/L K^+ buffer showed a negative Cotton effect at 242 nm and a positive one at 263 nm (Fig. 2B), thus confirming the presence of a parallel G4 structure (Supplementary data Fig. S3, green line). The addition of increasing amounts of porphyrin did not induce any change in the CD spectrum of **Q_1**, indicating that the binding with H_2TCPPSpm4 did not perturb the G4 structure. During the addition of porphyrin, a CD signal appeared in the 400–450 nm region, which could be ascribed to the interaction of H_2TCPPSpm4 with **Q_1**. Indeed, porphyrin is an achiral molecule and is silent to CD spectroscopy; however, after interacting with chiral species, CD signals can be induced (iCD) in the porphyrin absorption region. Moreover, it is known that the sign of the iCD profiles in the Soret region of porphyrin/nucleic acid complexes provides essential information about their interaction modes. As reported, a negative iCD band is produced upon intercalation or end-stacking of the porphyrin onto DNA sequence [39], a positive iCD band suggests a groove binding mode [41], and a bisegnate iCD profile indicates that porphyrins are orderly distributed onto the whole G4 structure communicating each other along the assembly [29]. Furthermore, a multisegnate iCD signal suggests the formation of π–π interactions between close porphyrins appended to a chiral scaffold with restricted conformational flexibility [42]. The CD spectrum of H_2TCPPSpm4/**Q_1** (1:1 ratio, Fig. 2B) showed a negative band centered at around 425 nm. This result, in agreement with the UV data, supports the hypothesis that the porphyrin at the 1:1 ratio binds **Q_1** by end-stacking. At the 2:1 ratio, the iCD profile showed a bisegnate signal with a negative iCD band centered at 421 nm and a positive one at 432 nm. According to the observed significant hypochromicity (62 %), this finding strongly indicated an end-stacking interaction of porphyrins with strong π-π interactions between them. At the 3:1, 4:1, and 5:1 H_2TCPPSpm4/**Q_1** ratio, trisegnate iCD signals with two negative bands at 406 nm and 442 nm and one positive band at 428 nm appeared, thus indicating the occurrence of strong π-π interactions among the porphyrin core of G4-bound H_2TCPPSpm4 molecules, which were indicative of the formation of high molecular weight H_2TCPPSpm4/**Q_1** aggregates.

2.2.3. Nondenaturing polyacrylamide gel electrophoresis (PAGE)

We used non-denaturing PAGE to compare the electrophoretic mobility of the H_2TCPPSpm4/**Q_1** complexes obtained at the 1:1 and 2:1 ratio (lanes 2 and 3, respectively, Fig. 2C) with that of **Q_1** alone (lane 1). In lane 1, we observed one clear band corresponding to the tetramolecular monomeric G4 **Q_1**. At the 1:1 ratio (lane 2), we observed the presence of two bands, the faster attributable to **Q_1** and the slower (**Q_X**) having gel mobility corresponding to about 45 base pairs (90 nt). The pale pink color of the slower **Q_X** band observed under 365 nm light allowed us to attribute the **Q_X** band to a porphyrin/**Q_1** complex rather than to a **Q_1** multimer. Moreover, the presence of multiple positive charges in H_2TCPPSpm4 reduces the net negative charge of the H_2TCPPSpm4/**Q_1** complex, decreasing the band mobility [43,44]. The addition of a second equivalent of the porphyrin derivative (2:1 ratio, lane 3) determined the disappearance of all bands under 254 and 365 nm illumination. This behavior agreed with the formation of supramolecular porphyrin-induced aggregates that did not migrate along the PAGE.

2.2.4. Resonance light scattering (RLS) studies

The binding mode of H_2TCPPSpm4 with **Q_1** was also investigated using resonance light scattering (RLS) measures. The RLS technique is precise in detecting the aggregation of chromophores [45,46]. The RLS spectra of the sole H_2TCPPSpm4 at 0.5–5.0 μmol/L concentrations are reported in Fig. S4 (Supplementary data). We observed that the RLS intensity increased linearly with the increase of the porphyrin concentration, thus suggesting the tendency of H_2TCPPSpm4 to self-assembly. However, the shape and intensity of the RLS signals did not agree with the occurrence of intense aggregation phenomena but rather were indicative of the formation of small aggregates. The RLS spectrum of H_2TCPPSpm4/**Q_1** complexes at the 1:1 ratio is less intense than that corresponding to the same amount of pure H_2TCPPSpm4 (Supplementary data, Fig. S5), thus indicating that the interaction with **Q_1** reduces the aggregation state of the porphyrin. At the 2:1 ratio, the RLS spectrum became almost superimposable with that of the porphyrin alone, thus indicating that some electronic communication between the G4-bound porphyrins occurred (Supplementary data Fig. S5). The RLS titration of a 2 μmol/L solution of **Q_1** with increasing concentrations of H_2TCPPSpm4 is reported in Fig. S6 (Supplementary data). By plotting the RLS intensity values at 455 nm (Supplementary data, inset Fig. S6), we observed two breakpoints at the 1:1 and 2:1 ratio that confirmed the formation of two different complexes in close agreement with the above-reported UV experiments. At a higher porphyrin/G4 ratio, we observed a linear increase of the RLS signal at 455 nm, which was comparable to that observed for the porphyrin alone, thus suggesting that no further interaction occurred between the porphyrin and the G4 model.

2.2.5. Fluorescence studies

We performed fluorescence measurements to determine the binding mode (external vs intercalation) of H_2TCPPSpm4 with the **Q_1** G4 model. Generally, external binding modes enhance the emission intensity of fluorescent chromophores, owing to a decrease in vibrational freedom. On the contrary, intercalation usually leads to emission quenching [29]. The fluorescence spectra of H_2TCPPSpm4 alone (0.5–5.0 μmol/L; λ_{exc} = 420 nm) showed two broad bands centered at 660 nm and 720 nm (Supplementary data Fig. S7). At the 1:1 H_2TCPPSpm4/**Q_1** ratio

(Supplementary data Fig. S8A), the spectrum shape evolved into two well-resolved and more intense vibrational bands, suggesting that each porphyrin molecule interacts with **Q_1** by end stacking at one of the two terminal faces of the G4 stem and did not interact with the others. This hypothesis agrees with previous findings, which excluded the intercalation binding mode between porphyrins and G4s composed of three or four G-tetrads [29]. Moreover, it is well known that stabilizing monovalent alkaline cations within the G4 stem hampers the intercalation binding mode [47–49]. We observed augmented fluorescence also at the 2:1 H_2TCPPSpm4/**Q_1** ratio (Supplementary data Fig. S8B), even if the enhancement of the two fluorescent signals was lower than that observed in the 1:1 ratio. This could be explained by hypothesizing that at the 2:1 ratio, some added porphyrins bind the porphyrin-free **Q_1** face and start communicating through long-distance exciton coupling with the porphyrin molecule stacked on the opposite face of the G4 stem, thus producing a partial signal quenching. At the 3:1 H_2TCPPSpm4/**Q_1** ratio, the fluorescence intensity decreased further (Supplementary data Fig. S8C), resulting in quenched signals compared to those of the porphyrin alone, probably because of the formation of longer H_2TCPPSpm4/**Q_1** nanoaggregates, supported by the trisegnate iCD signal at porphyrin/**Q_1** ratio $\geq$ 3:1 (Fig. 2B), in which the electronic coupling among G4-bound porphyrin molecules is maximized.

2.2.6. NMR studies

^{1}H NMR studies can offer significant indications of the binding events between G4 structures and their putative ligands. Porphyrin ligands' aromatic ring current produces substantial shifts in the G4 imino and aromatic protons neighboring the binding site. As shown in Fig. 3A, the water-suppressed ^{1}H NMR spectrum of the d(TGGGGT)$_4$ G4 structure showed a set of four exchangeable-protected N-1 imino protons signals in the range 11.6–10.9 ppm, each accounting for one of the four **Q_1**'s G-tetrads, as reported in previous papers [50]. Four additional imino proton signals (labeled with the # symbol) were also visible due to a second minor different G4 arrangement. The addition of one equivalent of H_2TCPPSpm4 to **Q_1** resulted in the appearance of the new set of signals labeled with asterisks (11.5–10.4 ppm) and the one labeled with the double dagger (9.5 ppm), respectively attributable to the upfield-shifted G-tetrads imino protons and the porphyrin amino protons in the 1:1 porphyrin/**Q_1** complex. Surprisingly, the addition of a second equivalent of porphyrin resulted in the disappearance of all imino and amino proton signals. This behavior can be attributed to the precipitation of the sample, which was observed by the naked eye in the NMR tube, due to the formation of insoluble H_2TCPPSpm4/**Q_1** aggregates at the 1 mmol/L ODN single strand concentration used for the NMR study. The number of G-tetrad imino proton signals in Fig. 3B and the porphyrin-induced Δδ values for these protons agree with the formation of a 1:1 H_2TCPPSpm4/**Q_1** complex in which the porphyrin molecule is stacked on top of the 3′ face of **Q_1**. The preference of binding for the **Q_1**'s 3′ end over its 5′ end can be attributed to the lower stability of the 5′-ending G2 tetrad (less intense and broader NMR signal for G2 imino protons at 11.6 ppm compared to G5 signals at 10.9 ppm) that would result in weaker π-π stacking interactions with the planar aromatic core of H_2TCPPSpm4. The NMR data strongly agreed with the PAGE, UV, and fluorescence results, pointing at the formation of the 1:1 complex at the 1:1 porphyrin/**Q_1** ratio and aggregates at higher porphyrin/G4 ratios.

2.2.7. Atomic force microscopy (AFM)

Atomic force microscopy (AFM) is one of the most potent tools for label-free nanoscale characterization of DNA-based supramolecular structures. It can help to characterize the size and shape of nanoaggregates or supramolecular structures resulting from the interaction of porphyrins with G-quadruplexes [51–54]. In this work, we used this technique to investigate the possible formation of supramolecular structures resulting from the adhesion of porphyrin/G4 complexes on the mica surface. Furthermore, the AFM analysis could confirm the presence of supramolecular aggregates not detectable by PAGE and NMR analyses, for example, because of their high molecular weight or

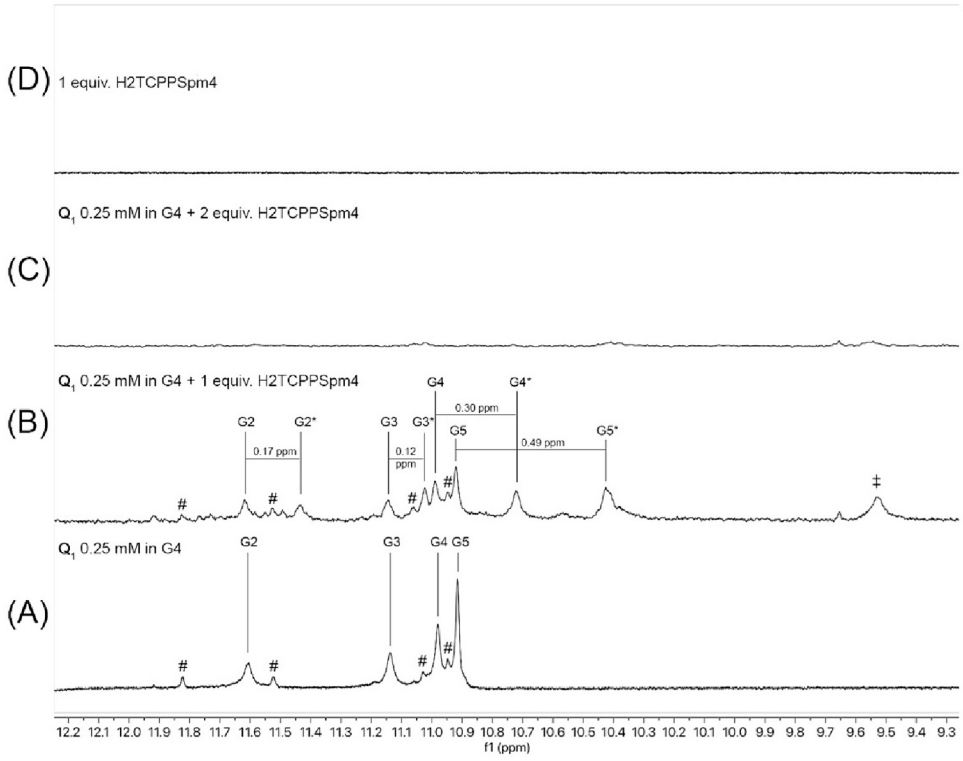

Fig. 3. Downfield region of the water-suppressed NMR spectra of: (A) d(TGGGGT)$_4$ (**Q_1**) annealed in 100 mmol/L K^+ buffer; (B) **Q_1** after the addition of 1 equiv. of H_2TCPPSpm4; (C) **Q_1** after the addition of 2 equiv. of H_2TCPPSpm4; (D) the sole H_2TCPPSpm4 in 100 mmol/L K^+ buffer. All spectra were recorded at 25 °C.

precipitation. Fig. 4 shows the AFM characterization of the **Q_1** G4 structures before and after their incubation with increasing amounts of H_2TCPPSpm4. In the case of the **Q_1** sample (Fig. 4, Panel 1), we observed aggregates of 2.6 ± 0.6 nm height, in agreement with the range of heights reported in the literature for G4s (1.5–3.5 nm), and 60 ± 20 nm width, a higher value than the expected 2 nm that can be attributed to the curvature radius of the AFM tip and the evaporation of the buffer solution both affecting the length and width measurements. When the **Q_1** sample was incubated with 1 equiv. of H_2TCPPSpm4 (Fig. 4, Panel 2), we observed two populations having different adsorption morphologies: (A) a set of nanostructures having an average height of 2 ± 1 nm and length/width of 60 ± 20 nm, attributable to the porphyrin free **Q_1** G4s; (B) nanowire-like structures having the same average height of 2 ± 1 nm and length of 340 ± 20 nm. In the case of incubation with 2 equiv. of porphyrin (Fig. 4, Panel 3), we observed randomly oriented rod-shaped structures having higher average lengths but preserving the same average height of 2.5 ± 0.5 nm. These results confirmed that the end stacking of H_2TCPPSpm4 at the 3′ and 5′ termini of **Q_1** promotes the formation of monolayer multimeric aggregates having different lengths, likely formed by porphyrin-mediated end-to-end stacking of different G4 building blocks.

2.3. Interaction of H_2TCPPSpm4 with the dimeric $[d(CGGAGGT)_4]_2$ G4 model (**Q_2**)

2.3.1. UV–Vis studies

We report in Fig. 5A the intensity of the Soret band absorbance (414 nm) of different concentrations of H_2TCPPSpm4 alone (red line) and in the presence of the dimeric G4 model $[d(CGGAGGT)_4]_2$ (**Q_2**) (blue line) plotting the A_{414} absorbance values versus the H_2TCPPSpm4/**Q_2** ratio. The alignment of all values along the blue line revealed that H_2TCPPSpm4 interacted with **Q_2** using the same binding mode at all the tested porphyrin/G4 ratios. The % of Δ slopes (Supplementary data Fig. S9B) confirmed the absence of breakpoints, showing values under 10 %, up to 4 equiv. of added porphyrin. In addition, unlike what was observed in the interaction with **Q_1**, the slope of the blue line did not become parallel to that of H_2TCPPSpm4 alone. At 1:1, 2:1, and 3:1 H_2TCPPSpm4/**Q_2** ratio, we observed an 8 nm red shift of the Soret band and a hypocromicity value under 30 % compared to the A_{414} values of H_2TCPPSpm4 alone at the same concentration (Supplementary data Fig. S9A–C). These findings suggested that H_2TCPPSpm4 interacted with **Q_2** through a unique external binding mode, i.e., into the grooves (lateral) or by end-stacking on the accessible 3′-ending faces of the G4 dimer. Differently from **Q_1**, the analysis of the Soret band hypochromicity at increasing porphyrin/**Q_2** ratio did not allow us to rule out the end-stacking binding mode because of the longer distance between the two 3′-ending faces of **Q_2** (~4.5 nm vs 2.2 nm).

2.3.2. CD studies

The CD profile of **Q_2** alone showed two negative bands at 225 and 285 nm and a positive band at 260 nm (Supplementary data Fig. S10, green line), thus confirming its 5′-5′ end-stacked dimeric G4 architecture [33]. The CD spectra recorded after the addition of increasing amounts of H_2TCPPSpm4 to **Q_2** are reported in Fig. 5B. At the 1:1 and 2:1 H_2TCPPSpm4/**Q_2** ratio, we observed a weak negative signal in the Soret region around 420 nm (inset Fig. 5B). At the 3:1 ratio, the iCD profile showed the transition from the negative iCD signal to a weak bisegnate signal. Further addition of porphyrin (4:1 and 5:1 ratio) enhanced the bisegnate signal with a negative iCD band at 444 nm and a positive one at 431 nm. Considering these data, we hypothesize that in the 1:1–3:1 porphyrin/**Q_2** ratio interval, one H_2TCPPSpm4 molecule binds one of the two G4 building blocks of the **Q_2** dimeric G4 model as a groove-binding ligand. In contrast, at porphyrin/**Q_2** ratios ≥3:1, the binding of a second porphyrin molecule at the other G4 building block occurs. This structural hypothesis agreed well with the NMR evidence discussed in Section 2.3.6, which excluded the end-stacking binding mode.

2.3.3. Nondenaturing polyacrylamide gel electrophoresis (PAGE)

We compared the PAGE mobility of the H_2TCPPSpm4/**Q_2** complexes formed at the 1:1, 2:1, and 3:1 ratio (lanes 3–5), respectively (Fig. 5C), with that of **Q_2** alone (lane 2). The PAGE bands were visualized by UV irradiation at 254 nm (left image) and 365 nm (right image). As expected, **Q_2** alone (56 nucleotides) migrated as a single band with mobility of about 25–30 bp of the DNA ladder (lane 1). The mixture H_2TCPPSpm4/**Q_2** at the 1:1 ratio (lane 3) led to a slower band (**Qy**, >50 bp) and a residual **Q_2** band. The addition of further amounts of

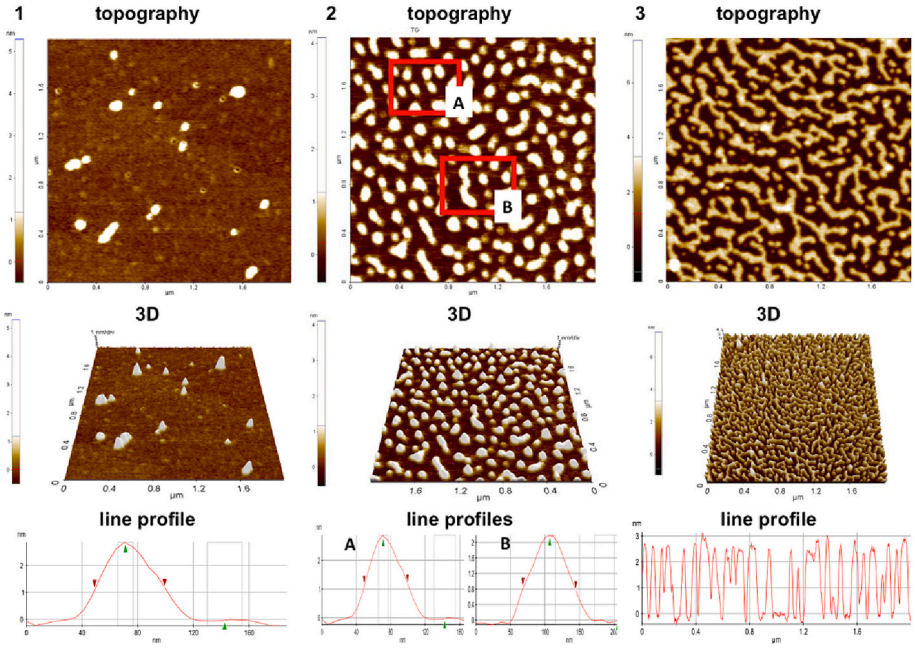

Fig. 4. AFM topography (top), three-dimensional rendering (middle), and a representative line profile (bottom) of pure **Q_1** (Panel 1) and **Q_1** with 1 equiv. (Panel 2) or 2 equiv. (Panel 3) of porphyrin. On the left of each AFM image, the color scale reports the respective height distribution where the darkest pixels are the lowest and the brightest ones are the highest, respectively.

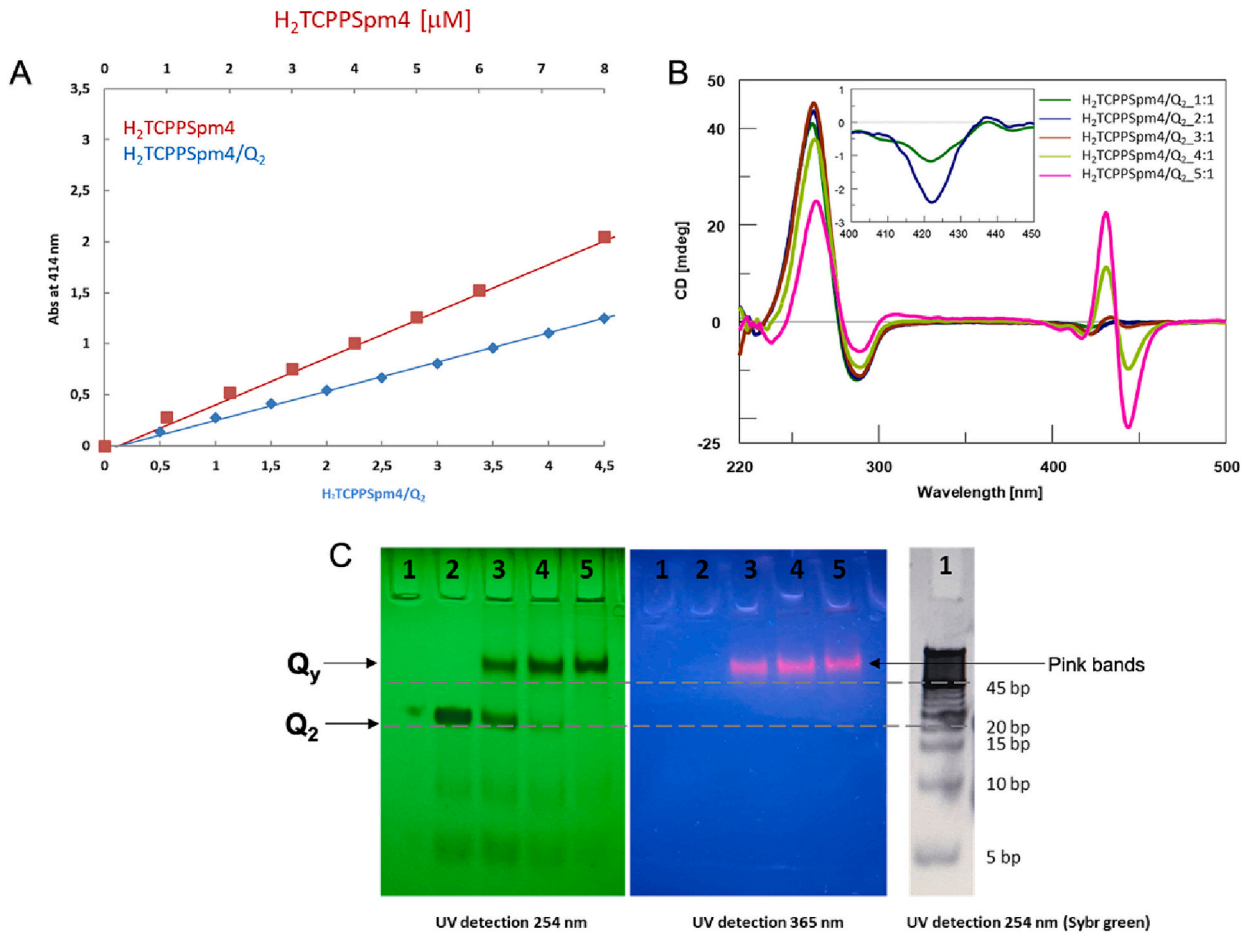

Fig. 5. (A) Soret band plot (414 nm) of increasing concentrations of H_2TCPPSpm4 alone (red line) and in the presence of the **Q_2** G4 model. (B) CD spectra of H_2TCPPSpm4/**Q_2**, from 1:1 to 5:1 ratio. Inset: H_2TCPPSpm4/**Q_2** at the 1:1 and 2:1 ratio. (C) PAGE images (UV–Vis lamp 254 nm and 365 nm); the DNA ladder (5–100 bp, lane 1) was visualized by Sybr green staining and UV transilluminator. Lane 2: $[d(CGGAGGT)_4]_2$ (**Q_2**); lanes 3–5: H_2TCPPSpm4/**Q_2** at the 1:1, 2:1, and 3:1 ratio, respectively. For non-processed PAGE images, refer to Fig. S18 (Supplementary data). (For interpretation of the references to color in this figure legend, the reader is referred to the web version of this article.)

porphyrin (2:1 and 3:1 ratio, lanes 4 and 5, respectively) led to the disappearance of the **Q_2** band and the increase of the intensity of the slower **Qy** band. The same gel visualized by UV light at 365 nm showed well-defined pink bands whose mobility matched that of the slower **Qy** band, thus confirming the presence of at least one porphyrin molecule in the **Qy** complex. In the light of further PAGE data (Supplementary data Fig. S20), which showed the presence of an additional band (**Q_2***) with mobility in between the **Q_2** and **Qy** bands, we believe that the **Qy** band can be attributed to an H_2TCPPSpm4/**Q_2** complex in which two porphyrin molecules are bound to the dimeric G4. In contrast, only one porphyrin ligand is present in the complex responsible for the appearance of the **Q_2*** band. Interestingly, more significant excesses of porphyrins (up to the 5:1 ratio) did not result in the appearance of any additional slower band than **Qy**.

2.3.4. RLS studies

The RLS spectra performed on H_2TCPPSpm4/**Q_2** samples prepared at the 1:1 and 2:1 ratio showed a linear increase of intensity up to the 2:1 ratio (Supplementary data Fig. S11). The absence of breakpoints up to the 2:1 ratio indicated that the binding mode of H_2TCPPSpm4 with **Q_2** did not change. These findings suggest that the two porphyrins in **Q_2** are far enough apart to prevent communication between them. The RLS intensity increased at the 3:1 H_2TCPPSpm4/**Q_2** ratio, thus indicating that porphyrin-porphyrin interactions between H_2TCPPSpm4 molecules belonging to different H_2TCPPSpm4/**Q_2** complexes could occur.

2.3.5. Fluorescence studies

The fluorescence spectra of H_2TCPPSpm4/**Q_2** complexes obtained at the 1:1 and 2:1 ratio (Supplementary data Fig. S12A–B) showed two well-resolved vibrational bands centered at 660 nm and 720 nm, with intensities higher than those of the corresponding bands of porphyrin alone. These results indicate a decreased vibrational freedom of porphyrin molecules in the 1:1 and 2:1 mixtures with **Q_2**, probably due to the strong binding on **Q_2**. These results agree with the structural hypotheses suggested by CD data. The fluorescence spectrum recorded at the 3:1 ratio (Supplementary data Fig. S12C) showed two well-resolved bands having intensities higher than those of the corresponding bands of porphyrin alone but lower than those observed for the spectrum obtained at the 2:1 ratio. This data suggests that the porphyrins added with the third equivalent could be involved in stacking interactions with the porphyrins located in the grooves of the G4 stem, thus inducing a partial quenching of fluorescence, in agreement with the RLS data.

2.3.6. NMR studies

The downfield region of the NMR spectra of the G-quadruplex dimer **Q_2** registered before and 10 min after each addition of one to three equivalents of H_2TCPPSpm4 are reported in Fig. 6A–D. As reported by some of us in a previous paper [33], the NMR spectrum of **Q_2** showed four well-resolved N-1 imino protons signals in the range 11.5–10.3 ppm, which were assigned to the four G-tetrads in each of the two magnetically equivalent G-quadruplexes constituting the **Q_2** dimer, and

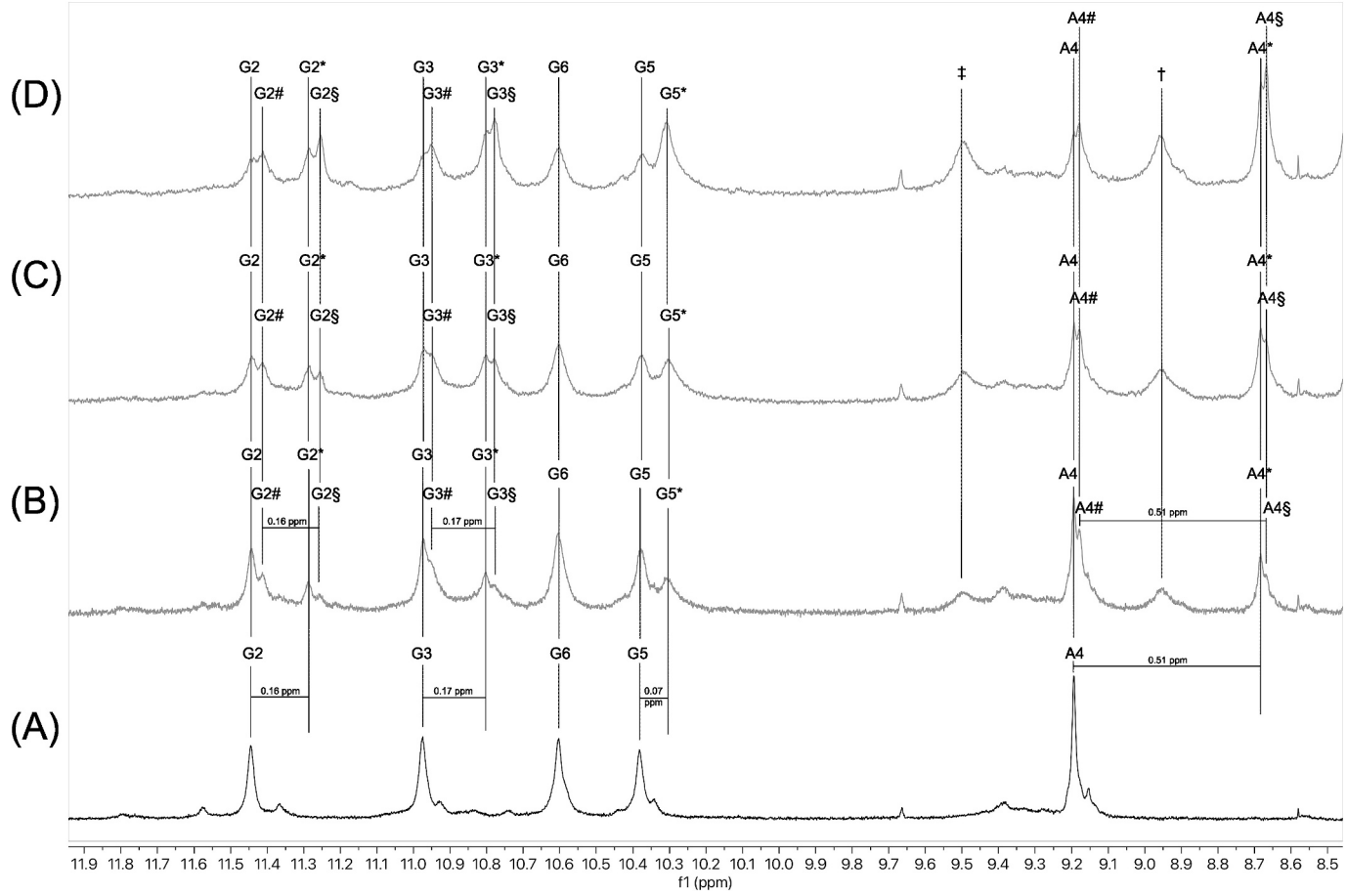

Fig. 6. Downfield region of the water-suppressed NMR spectra of: (A) $[d(CGGAGGT)_4]_2$ (**Q_2**) annealed in 100 mmol/L K^+ buffer and recorded at 25 °C; (B–D) **Q_2** after the addition of 1 (B), 2 (C), and 3 (D) equiv. of H_2TCPPSpm4.

one sharp signal at 9.2 ppm which was attributed to the downfield-shifted H2 proton of A bases engaged in A-tetrad formation [55]. The addition of one equivalent of H_2TCPPSpm4 to **Q_2** caused the appearance of three new sets of upfield-shifted imino proton signals labeled with *, #, and §, which confirmed the interaction between the G4 dimer and the porphyrin, together with the signals resonating at 8.9 (labeled with †) and 9.5 (labeled with ‡) that were attributed to the porphyrin's β-pyrrole and amino hydrogens, respectively. The addition of a second equivalent of porphyrin determined the reduction in the intensity of all imino proton signals of the porphyrin-free **Q_2** and the concomitant enhancement of signals belonging to the *, #, and § series (Fig. 6C). The addition of the third equivalent of porphyrin resulted in the further enhancement of signals belonging to the * and § series, with the latter series become the most intense (Fig. 6D). The number and intensity of imino and A4-H2 proton signals during the titration with the porphyrin agreed with the formation of two different complexes characterized by the 1:1 (accounting for signals labeled with the * and # symbols) and the 2:1 (accounting for signals labeled with the § symbol) porphyrin/**Q_2** ratio. We hypothesize that the binding of the first porphyrin molecule to one of the two G4 units in **Q_2** determines the breaking of the magnetic equivalence of the two G-quadruplex units due to the upfield shifting of almost all imino and A4-H2 protons both in the porphyrin-bound (* series) and the porphyrin-unbound (# series) G-quadruplex unit that was inversely proportional to the distance of each proton from the porphyrin ring current. The analysis of the Δδ value of proton signals belonging to the * series relative to the corresponding signals of **Q_2** alone (Fig. 6B) indicates the A4-H2 protons as the most perturbed protons (Δδ = 0.51 ppm) and the G6 imino protons as the least perturbed one (Δδ ≅ 0 ppm), thus suggesting that H_2TCPPSpm4 interacts with **Q_2** as a G-quadruplex groove-binder rather than as an end-stacking ligand as we found for the 1:1 H_2TCPPSpm4/**Q_1** complex. More specifically, the absolute value of the Δδ shift of A4-H2 protons resulted similar to that reported for the formation of the A-tetrad in other G-quadruplexes [55], thus indicating that the external binding of the porphyrin with the G-quadruplex groove disrupted the central A-tetrad causing the 0.51 ppm upshift of A4-H2 protons because of their displacement from the N7 atom of the flanking A nucleobase. This hypothesis was further supported by the analysis of the Δδ values of protons belonging to the § series relative to the corresponding protons of the # series, which resulted to be identical to those found for protons belonging to the * series relative to those of the bare **Q_2** (Fig. 6A–B). In other words, the binding of the second porphyrin molecule to the ligand-free G4 unit in the 1:1 H_2TCPPSpm4/**Q_2** complex followed the same binding mode of the first one, determining the "# to §" proton signals transition, as well as the contextual "* to §" transition for protons belonging to the porphyrin-bound G4 unit. These findings fully agree with the UV titration data, which accounted for a single groove binding mode.

2.3.7. *AFM studies*

Fig. 7 shows the AFM characterization of **Q_2** structures before and after H_2TCPPSpm4 addition. In the case of **Q_2** alone (Fig. 7, Panel 1), we observed some nanostructures whose heights are distributed around an average value of 3.0 ± 0.6 nm, corresponding to the height value of the **Q_2** building block, which has a height almost identical to the **Q_1** building block. The lengths of the observed nanostructures for **Q_2** are distributed around 130 ± 40 nm. Also in this case, we measured length values significantly higher than those expected, in agreement with what was observed and discussed in the case of **Q_1** (Section 2.2.7). Moreover, most

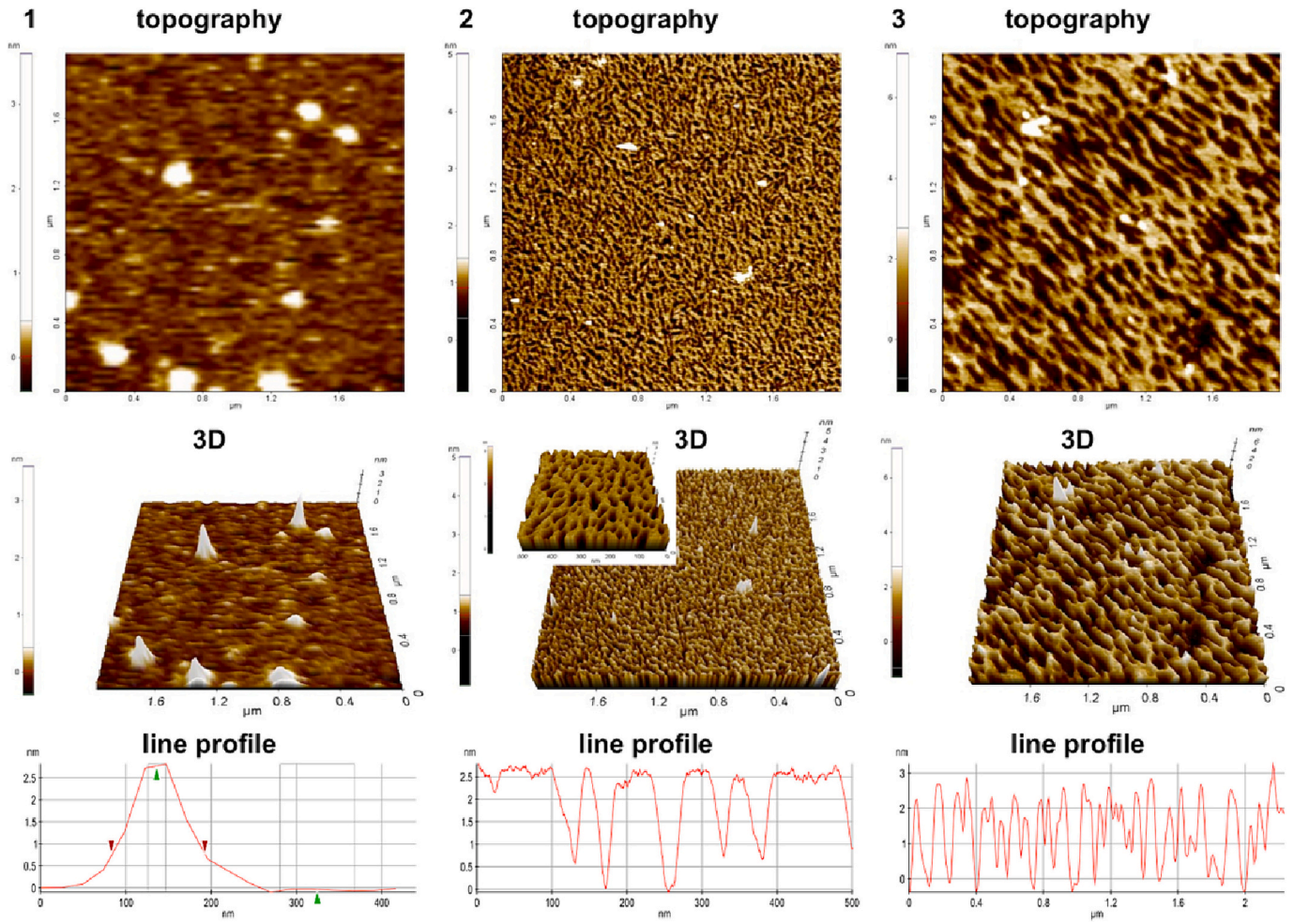

Fig. 7. AFM topography (top), three-dimensional rendering (middle), and a representative line profile (bottom) of pure **Q_2** sample (Panel 1) and **Q_2** with 1 equiv. (Panel 2) or 3 equiv. (Panel 3) of H_2TCPPSpm4. On the left of each AFM image, the color scale reports the respective height distribution, where the darkest pixels are the lowest, and the brightest ones are the highest, respectively.

of the pixels in Fig. 7 (Panel 1) have height values lower than 0.5 nm, attributable to the surface roughness of mica. This evidence highlights that only a few **Q_2** structures were bound to the mica surface due to a weak interaction with the mica substrate. On the contrary, after the addition of 1 equiv. and 2 equiv. of porphyrin (Fig. 7, Panels 2 and 3, respectively), most of the pixels have a height higher than 2 nm, suggesting that the formation of H_2TCPPSpm4/**Q_2** complexes having a higher affinity with the mica surface takes place. In the case of H_2TCPPSpm4/**Q_2** complexes formed at the 1:1 ratio (Fig. 7, Panel 2), we observed a dense and thin net of the cross-linked aggregate layer of 2.6 ± 0.1 nm height, which becomes less dense and less thin when a second equivalent of H_2TCPPSpm4 was added (2.2 ± 0.6 nm height) (Fig. 7, Panel 3). These results suggested that the binding of porphyrin molecules externally on the **Q_2** G4 rods leads to the formation of a cross-linked monolayer by lateral side packing of H_2TCPPSpm4/**Q_2** complexes when adsorbed on mica.

*2.4. Interaction of H_2TCPPSpm4 with the multimeric [d(5′-CGGT-3′-3′-GGC-5′)$_4$]$_n$ G4 model (**Q_n**)*

Usually, DNA G-wires are formed by the cooperative binding of four G-rich slipped DNA strands held together by G-tetrads formation, thus creating very stable long G4 rods known as interlocked G-wires [56–58], or by π-π stacking of preformed monomolecular G4 units [6,59]. The interaction study of interlocked DNA G-wires with the tetracationic porphyrin TMPyP4 has been reported, defining the binding mode of the porphyrin and possible application in nanomaterials [56,57]. Our G-wire model **Q_n** (Fig. 1) is formed by the axial attachment of tetramolecular G4 entities held together by π-π stacking interactions between planar C-G octads at their 5′ termini [34,35]. This type of G-wire assembly is less stable compared to the interlocked G-wires, but, at least in principle, its multimerization process and interaction with specific ligands could be better controlled to achieve G-wires having governable length and new chemical physical properties. The number of the constituting G4 units in the **Q_n** model can be estimated using PAGE (Fig. 8C) and HPLC SEC chromatography [34,35,60].

2.4.1. UV–Vis studies

In Fig. 8A, we report the intensity of the absorbances of the Soret band (A_{414} nm) of H_2TCPPSpm4 alone at different concentrations (red line) and in the presence of **Q_n** (blue line). For the H_2TCPPSpm4/**Q_n** mixture, the blue line connecting the absorbance values did not show any distinct breakpoint, thus indicating that the porphyrin interacted with **Q_n** at all tested concentrations using a single binding mode. The % of Δ slopes, showing values under 10 % up to 4 equiv. of added porphyrin, confirmed the absence of breakpoints (Supplementary data Fig. S13B). The almost parallel trend of the red and blue lines in Fig. 8A suggested that only slight interactions between H_2TCPPSpm4 and **Q_n** occurred. Indeed, the UV spectrum of H_2TCPPSpm4/**Q_n** at the 1:1 ratio showed no shift of the Soret band at 414 nm, the appearance of a low shoulder at 425 nm, and a low hypocromicity value (18 %) compared to the porphyrin alone (Supplementary data Fig. S13). By raising the

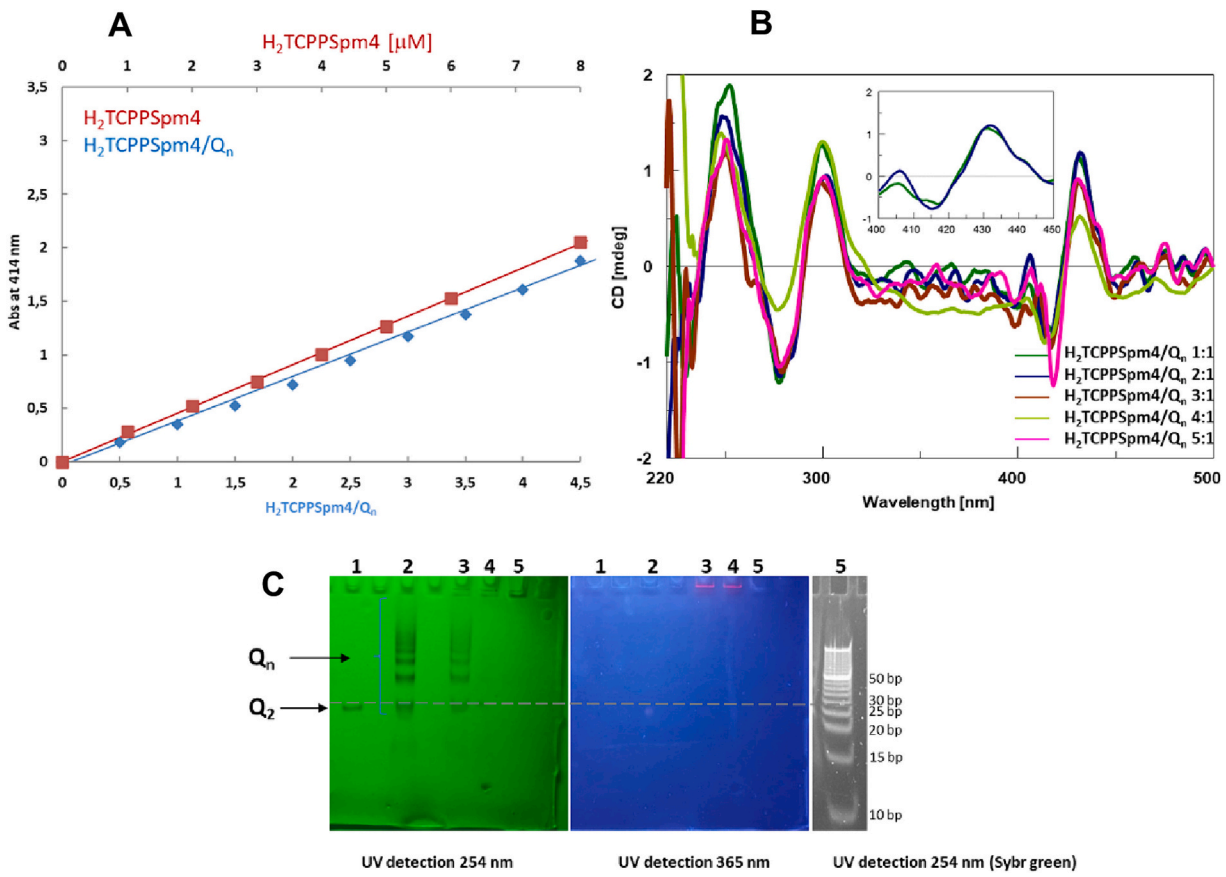

Fig. 8. (A) Soret band plot (414 nm) of increasing concentrations of H_2TCPPSpm4 alone (red line) and in the presence of the **Q_n** G4 model (blue line). (B) CD spectra of H_2TCPPSpm4/**Q_n**, from 1:1 to 5:1 ratio; inset: H_2TCPPSpm4/**Q_2** at the 1:1 and 2:1 ratio. (C) PAGE images (UV–Vis lamp 254 nm and 365 nm); the DNA ladder (lane 5) was visualized by Sybr green staining and UV transilluminator (10–100 bp); lane 1: **Q_2**; lane 2: $[d(5'\text{-CGGT-}3'\text{-}3'\text{-GGC-}5')_4]_n$ (**Q_n**); lanes 3 and 4: H_2TCPPSpm4/**Q_n** at the 1:1 and 3:1 ratio, respectively. For non-processed PAGE images, refer to Fig. S19 (Supplementary data). (For interpretation of the references to color in this figure legend, the reader is referred to the web version of this article.)

amount of the porphyrin at the 2:1 and 3:1 ratios, we observed the disappearance of the shoulder at 425 nm and the increase of the hypochromic effect at 28 % and 35 %, respectively. These findings indicated that H_2TCPPSpm4 interacted with the **Q_n** G-wire as a groove-binding ligand. However, differently from what we observed in the interaction with **Q_1**, we cannot exclude the end-stacking binding to the two terminal 5′ faces of each **Q_i** member of the **Q_n** distribution because the UV contribution of such interaction would be negligible, both in terms of Soret band shift and hypochromicity, for this type of longer G4 assembly.

2.4.2. CD studies

The CD profile of **Q_n** (Supplementary data Fig. S14) shows a positive CD signal at 245 nm, a negative band around 280 nm, and a second positive signal at 300 nm, as previously described [35]. After the addition of increasing amounts of porphyrin, from 1:1 to 5:1 ratio, the CD spectra of H_2TCPPSpm4/**Q_n** resulted almost superimposable to that of the sole **Q_n** polymer (Fig. 8B). This behavior suggested that the incubation with the porphyrin did not significantly affect the structural features of the **Q_n** G-wire distribution. Furthermore, one positive iCD signal at 431 nm and a negative one at 420 nm were also detected. These iCD signals did not change in shape and intensity with different H_2TCPPSpm4 concentrations, thus supporting the hypothesis that the same binding mode occurred at all the tested porphyrin concentrations.

2.4.3. PAGE analyses

In Fig. 8C, we report the PAGE mobility of the H_2TCPPSpm4/**Q_n** mixture at the 1:1 and 3:1 ratio (lanes 3 and 4, respectively) compared with those of the G4 dimer **Q_2** (lane 1) and pure **Q_n** (lane 2). The latter, as expected, migrated as a distribution of multimeric G4 species formed by stacked tetramolecular G4 blocks. In the presence of 1 equiv. of H_2TCPPSpm4 (1:1 ratio, lane 3), we observed almost the same electrophoretic mobility as the pure **Q_n** mixture and a slight reduction in the intensity of all bands. It is to be noted that 1 equiv. of porphyrin is calculated as one-fourth of the ODN single strand (**3**) used to obtain **Q_n**, so the 1:1 ratio ensured the presence of at least one porphyrin molecule for each G4 building block. In this way, two porphyrin molecules were available for block **Q_2**, three for **Q_3**, and so on for longer **Q_n** multimers. The incubation of **Q_n** with 3 equiv. of H_2TCPPSpm4 (3:1 ratio, lane 4) determined the disappearance of all PAGE bands (detection at 254 nm). The pink band localized at the bottom of the loading well of lanes 3 and 4 revealed the presence of porphyrin molecules that did not migrate in the gel, probably being part of supramolecular porphyrin/G4 aggregates.

2.4.4. RLS studies

The RLS spectra of a 2 μmol/L solution of **Q_n** in the presence of increasing amounts of H_2TCPPSpm4 (from 0.5 to 8.5 μmol/L) are reported in Supplementary data Fig. S15. The spectra indicated the formation of large aggregates already after the addition of 1 equiv. H_2TCPPSpm4 (~720 a.u. intensity at 455 nm). Moreover, the linear enhancement of the RLS intensity at increasing porphyrin concentrations suggested that H_2TCPPSpm4 molecules are bound externally to the **Q_n** wire using a single binding mode at all the tested concentrations.

2.4.5. Fluorescence studies

Fluorescence spectra of H_2TCPPSpm4/**Q_n** species (Supplementary data Fig. S16) showed a reduction in the intensity of fluorescent bands centered at 660 nm and 720 nm compared to those of the sole porphyrin. This behavior is the opposite of that observed in the titration of **Q_2** and suggests that strong quenching phenomena occurred at all porphyrin concentrations tested. This quenching could be caused by porphyrin-porphyrin interactions among molecules bound in the grooves of the G-wire stem. Above all, the fluorescence data excluded a significative role of the 5′-stacking binding mode of H_2TCPPSpm4 on **Q_n** and suggested the occurrence of lateral interactions along the stem of the stacked G-wires.

2.4.6. AFM studies

Fig. 9 shows the AFM images of **Q_n** G-wires before and after the H_2TCPPSpm4 addition. In the case of the sole **Q_n** (Fig. 9, Panel 1), we observed long rods with different lengths (50–100 nm) having 2.5 ± 0.3 nm average height (see the representative line profile at the bottom of Fig. 9, Panel 1), corresponding to the height value of the G4 building block. In the presence of 1 equiv. of H_2TCPPSpm4, **Q_n** loses the ordered shape of nanowires to form fragmented structures – having variable length/width (50–200 nm) but preserving the typical height of G4 monolayers (2.0 ± 0.5 nm) – caused by lateral aggregation of G4-bound porphyrin molecules (Fig. 9, Panel 2). The addition of 3 equiv. of porphyrin to **Q_n** increased the amount and dimension of these aggregates. In particular, we observed that the average height of the H_2TCPPSpm4/**Q_n** aggregates deposited on the mica surface rose to 4.0 ± 2 nm (Fig. 9, Panel 3). These data suggested that the higher number of available porphyrins induces critical structural changes when the mixture is adsorbed on the mica surface, allowing the formation of multilayer G4 aggregates by lateral stacking interaction between porphyrins molecules located in the grooves of the G-wire rods. Finally, the AFM image of pure H_2TCPPSpm4 used as control (Supplementary data Fig. S17) confirmed that the adsorption of the sole H_2TCPPSpm4 molecules on the mica surface does not form nanostructures but only a thin layer of aggregates with a maximum height of 1 nm.

2.5. HPLC Size Exclusion Chromatography (SEC) analyses on Q_1, Q_2, and Q_n samples in the presence of H_2TCPPSpm4

The HPLC Size Exclusion Chromatography (SEC) is a well-established technique for determining the molecular weight and molecularity of G4s and their multimers [34,35,61–63]. As described above, in the presence of 1 equiv. of porphyrin **Q_1** formed a single H_2TCPPSpm4/**Q_1** complex visualized in the PAGE as the **Qx** band having significative lower mobility than the **Q_1** band (Fig. 2C). All the spectroscopic techniques suggested that **Qx** contained a porphyrin molecule stacked, most probably, on the 3′-ending face of the G4 stem as for the NMR findings. Here, we used HPLC-SEC to ascertain whether the slower **Qx** PAGE band was due to a porphyrin-bound G4 monomer with reduced net negative charge or a higher molecular weight porphyrin-bound G4 multimer. In the literature, many papers report the PAGE mobility of complexes formed between polycationic ligands and DNA duplexes or G4s. In those cases, conflicting results were reported – both no slowing and significative slowing of the complexes' bands were reported [22,44,63–65] – likely because polycationic molecules could be stripped away during the electrophoresis run, thus producing no changes in the PAGE mobility [43]. The HPLC SEC analyses of **Q_1** in the presence of 1–3 equiv. of H_2TCPPSpm4 demonstrated unambiguously that the porphyrin/**Q_1** complex (Supplementary data Fig. S22, detection at 414 nm) has almost the same retention time as **Q_1** (Supplementary data Figs. S21 and S22, detection at 260 nm), thus excluding the formation of porphyrin-induced **Q_1** multimers. The addition of the second and third equivalent of porphyrin to **Q_1** induced a substantial reduction in the peak intensity of **Q_1** and H_2TCPPSpm4/**Q_1** species, thus confirming the rapid formation of not detectable higher molecular weight aggregates at porphyrin/G4 ratios higher than 1:1.

The HPLC SEC analysis of **Q_2** following the incubation with 1–3

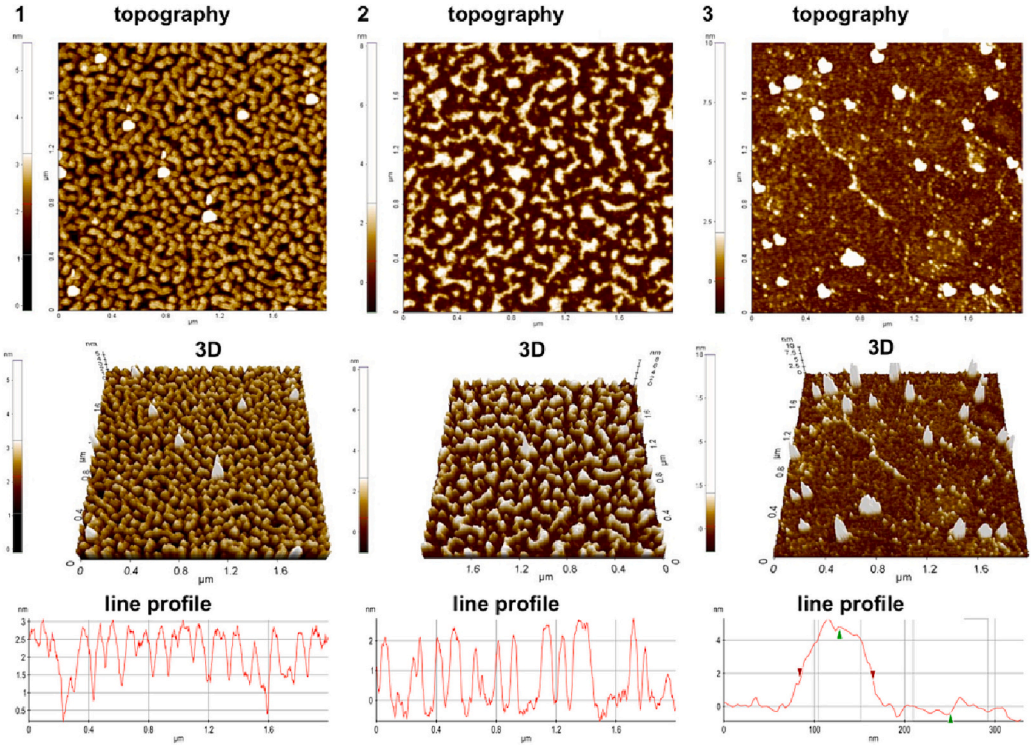

Fig. 9. AFM topography (top), three-dimensional rendering (middle), and a representative line profile (bottom) of pure **Q_n** sample (Panel 1) and **Q_n** with 1 eq. (Panel 2) or 3 equiv. (Panel 3) of porphyrin. On the left of each AFM image, the color scale reports the respective height distribution, where the darkest pixels are the lowest, and the brightest ones are the highest, respectively.

equiv. of H_2TCPPSpm4 (Supplementary data Fig. S23, detection at 414 nm) indicated the absence of H_2TCPPSpm4/**Q_2** multimers and the presence of a sole peak (**Qy**) with a retention time slightly higher than that of the sole **Q_2**, in close analogy with what observed for the complex formed between H_2TCPPSpm4 and the **Q_1** G4 model. This data demonstrated that the slower **Qy** band observed in the PAGE reported in Fig. 5C was due to a porphyrin-bound **Q_2** complex and not a porphyrin-bound **Q_2** multimer.

The results of the HPLC SEC analysis performed on **Q_n** after its incubation with 0.25–3 equiv. of H_2TCPPSpm4 are reported in Supplementary data Fig. S24. Before the addition of the porphyrin, the SEC profile of **Q_n** was populated by a distribution of peaks having different intensity and retention time (detection at 260 nm, blue line) accounting for the presence in the solution of the complete series of **Q_i** multimers and the single-stranded ODN **3** (t_R = 16.5 min). The addition of 0.25–1 equiv. of porphyrin determined a marked reduction in the intensity of all peaks, in close agreement with PAGE data (Fig. 5C, lane 3), because of the partial formation of supramolecular aggregates not revealable by the SEC analysis. Two interesting aspects could be noted by comparing the HPLC profiles detected at 260 and 414 nm. First, the addition of the porphyrin induced a not uniform reduction in peaks' intensity, with the shorter **Q_1** species resulting in the least affected; second, the absence of the peak belonging to the single-stranded **3** (i.e., the intense peak labeled with SS in the HPLC profile detected at 260 nm) in the HPLC profile detected at 414 nm revealed a strong binding selectivity of H_2TCPPSpm4 for the G4-folded ODN **3** versus its random coil conformation. Finally, the HPLC SEC profiles obtained after the addition of 3 equiv. of porphyrin did not show any significant peak when detected at 260 and 414 nm, thus confirming the complete formation of non-revealable supramolecular aggregates in agreement with PAGE and AFM results.

3. Conclusions

In conclusion, by using several complementary analytical techniques, we have studied the interaction between the cationic porphyrin H_2TCPPSpm4 and some representative parallel G-quadruplex models to define the binding mode and compare the data furnished by all techniques to delineate their strengths and limitations. The results revealed that H_2TCPPSpm4 can bind the G4 models by using either the end-stacking or the groove-binding modes, depending on the accessibility of the G4 ending faces and the length of the G4 stem. Specifically, we found that H_2TCPPSpm4 interacts with the shorter **Q_1** exclusively as an end-faces binder, with a marked selectivity towards the 3′-ending face that is the only one targeted at the 1:1 H_2TCPPSpm4/**Q_1** ratio. The addition of the second equivalent of porphyrin determines the binding at the opposite 5′-ending face, which in turn triggers the formation of more extended, insoluble G-wire aggregates that are undetectable by NMR, PAGE, and SEC but whose formation can be monitored by CD, RLS, and AFM. The elongation of the G-quadruplex forming ODN from six to seven nucleobases determined the switch from the end-stacking to the groove-binding mode, which was the sole one observed for the formation of H_2TCPPSpm4/**Q_2** and H_2TCPPSpm4/**Q_n** complexes. However, we observed an exciting different outcome when more than two equivalents were added to the **Q_2** or **Q_n** G4 model. As for the G4 dimer **Q_2**, we did not observe the formation of higher molecular weight aggregates than the 2:1 H_2TCPPSpm4/**Q_2** complex, as ascertained by PAGE and HPLC-SEC. Conversely, supramolecular, insoluble aggregates readily formed when three or more equivalents were added to the **Q_n** multimeric G4 model. This different behavior can be attributed to the higher number of porphyrin molecules bound in the G4 grooves of the latter model that maximizes the probability of the occurrence of porphyrin-porphyrin stacking interaction between H_2TCPPSpm4 molecules bound to different H_2TCPPSpm4/**Q_n** complexes. This study adds valuable insights to the understanding of mechanisms underlying the interaction between porphyrin-based ligands and DNA G-quadruplexes and the development of new porphyrin-based therapeutics or supramolecular biomaterials.

CRediT authorship contribution statement

Andrea Patrizia Falanga: Investigation, Methodology. **Alessandro D'Urso:** Investigation. **Gabriele Travagliante:** Formal analysis, Investigation. **Chiara Maria Antonietta Gangemi:** Formal analysis, Investigation. **Maria Marzano:** Investigation, Software. **Stefano D'Errico:** Investigation, Methodology. **Monica Terracciano:** Formal analysis. **Francesca Greco:** Data curation, Investigation. **Luca De Stefano:** Data curation. **Principia Dardano:** Data curation, Investigation. **Ilaria Rea:** Formal analysis, Methodology. **Gennaro Piccialli:** Data curation, Funding acquisition, Writing – original draft. **Giorgia Oliviero:** Conceptualization, Formal analysis, Methodology. **Nicola Borbone:** Conceptualization, Data curation, Investigation, Supervision, Writing – original draft, Writing – review & editing.

Declaration of competing interest

The authors declare no conflicts of interest.

Acknowledgements

Ministero dell'Università e della Ricerca [FOE 2020-ISBE-IT Joint Research Unit]. Part of the data reported in this paper was produced using the Infrastructure Services established as part of the project European Union NextGenerationEU [IR0000010 "ELIXIRxNextGenIT", PNRR MUR-M4C2—Investimento 3.1, CUP UNINA: B53C22001800006].

Appendix A. Supplementary data

Supplementary data to this article can be found online at https://doi.org/10.1016/j.ijbiomac.2024.131801.

References

[1] S. Burge, G.N. Parkinson, P. Hazel, A.K. Todd, S. Neidle, Quadruplex DNA: sequence, topology and structure, Nucleic Acids Res. 34 (2006) 5402–5415, https://doi.org/10.1093/nar/gkl655.
[2] H.L. Lightfoot, T. Hagen, N.J. Tatum, J. Hall, The diverse structural landscape of quadruplexes, FEBS Lett. 593 (2019) 2083–2102, https://doi.org/10.1002/1873-3468.13547.
[3] S. Kolesnikova, E.A. Curtis, Structure and function of multimeric G-Quadruplexes, Molecules 24 (2019) 3074, https://doi.org/10.3390/molecules24173074.
[4] S. Bag, M.D. Burman, S. Bhowmik, Structural insights and shedding light on preferential interactions of dietary flavonoids with G-quadruplex DNA structures: a new horizon, Heliyon 9 (2023) e13959, https://doi.org/10.1016/j.heliyon.2023.e13959.
[5] D. Pavc, B. Wang, L. Spindler, I. Drevenšek-Olenik, J. Plavec, P. Šket, GC ends control topology of DNA G-quadruplexes and their cation-dependent assembly, Nucleic Acids Res. 48 (2020) 2749–2761, https://doi.org/10.1093/nar/gkaa058.
[6] N. Smargiasso, F. Rosu, W. Hsia, P. Colson, E.S. Baker, M.T. Bowers, E. De Pauw, V. Gabelica, G-quadruplex DNA assemblies: loop length, cation identity, and multimer formation, J. Am. Chem. Soc. 130 (2008) 10208–10216, https://doi.org/10.1021/ja801535e.
[7] G. Oliviero, J. Amato, N. Borbone, A. Galeone, L. Petraccone, M. Varra, G. Piccialli, L. Mayol, Synthesis and characterization of monomolecular DNA G-quadruplexes formed by tetra-end-linked oligonucleotides, Bioconj. Chem. 17 (2006) 889–898, https://doi.org/10.1021/bc060009b.
[8] D. Rhodes, H.J. Lipps, G-quadruplexes and their regulatory roles in biology, Nucleic Acids Res. 43 (2015) 8627–8637, https://doi.org/10.1093/nar/gkv862.
[9] M. Scuotto, M. Persico, M. Bucci, V. Vellecco, N. Borbone, E. Morelli, G. Oliviero, E. Novellino, G. Piccialli, G. Cirino, M. Varra, C. Fattorusso, L. Mayol, Outstanding effects on antithrombin activity of modified TBA diastereomers containing an optically pure acyclic nucleotide analogue, Org. Biomol. Chem. 12 (2014) 5235–5242, https://doi.org/10.1039/C4OB00149D.
[10] C. Platella, C. Riccardi, D. Montesarchio, G.N. Roviello, D. Musumeci, G-quadruplex-based aptamers against protein targets in therapy and diagnostics, Biochim. Biophys. Acta Gen. Subj. 2016 (1861) 1429–1447, https://doi.org/10.1016/j.bbagen.2016.11.027.
[11] F. Nici, G. Oliviero, A.P. Falanga, S. D'Errico, M. Marzano, D. Musumeci, D. Montesarchio, S. Noppen, C. Pannecouque, G. Piccialli, N. Borbone, Anti-HIV

activity of new higher order G-quadruplex aptamers obtained from tetra-end-linked oligonucleotides, Org. Biomol. Chem. 16 (2018) 2349–2355, https://doi.org/10.1039/C7OB02346D.
[12] J. D'Onofrio, L. Petraccone, E. Erra, L. Martino, G. Di Fabio, L. De Napoli, C. Giancola, D. Montesarchio, 5′-Modified G-Quadruplex forming oligonucleotides endowed with anti-HIV activity: synthesis and biophysical properties, Bioconjug. Chem. 18 (2007) 1194–1204, https://doi.org/10.1021/bc070062f.
[13] K.-T.T. Shum, J. Zhou, J.J. Rossi, Aptamer-based therapeutics: new approaches to combat human viral diseases, Pharmaceuticals (Basel) 6 (2013) 1507–1542, https://doi.org/10.3390/ph6121507.
[14] B. Gatto, M. Palumbo, C. Sissi, Nucleic acid aptamers based on the G-quadruplex structure: therapeutic and diagnostic potential, Curr. Med. Chem. 16 (2009) 1248–1265, https://doi.org/10.2174/092986709787846640.
[15] D. Sen, W. Gilbert, Novel DNA superstructures formed by telomere-like oligomers, Biochemistry 31 (1992) 65–70, https://doi.org/10.1021/bi00116a011.
[16] J.E. Betancourt, J.M. Rivera, Tuning thermoresponsive supramolecular G-quadruplexes, Langmuir 31 (2015) 2095–2103, https://doi.org/10.1021/la504446k.
[17] D. Hu, J. Ren, X. Qu, Metal-mediated fabrication of new functional G-quartet-based supramolecular nanostructure and potential application as controlled drug release system, Chem. Sci. 2 (2011) 1356–1361, https://doi.org/10.1039/c1sc00109d.
[18] F. Simmel, W. Dittmer, D.N.A. Nanodevices, Small 1 (2005) 284–299, https://doi.org/10.1002/smll.200400111.
[19] E. Stulz, DNA architectonics: towards the next generation of bio-inspired materials, Chemistry 18 (2012) 4456–4469, https://doi.org/10.1002/chem.201102908.
[20] L.A. Yatsunyk, O. Mendoza, J.-L. Mergny, "Nano-oddities": unusual nucleic acid assemblies for DNA-based nanostructures and nanodevices, Acc. Chem. Res. 47 (2014) 1836–1844, https://doi.org/10.1021/ar500063x.
[21] P. Changenet-Barret, E. Emanuele, T. Gustavsson, R. Improta, A.B. Kotlyar, D. Markovitsi, I. Vayá, K. Zakrzewska, D. Zikich, Optical properties of guanine nanowires: experimental and theoretical study, J. Phys. Chem. C 114 (2010) 14339–14346, https://doi.org/10.1021/jp102106d.
[22] H. Han, D.R. Langley, A. Rangan, L.H. Hurley, Selective interactions of cationic porphyrins with G-quadruplex structures, J. Am. Chem. Soc. 123 (2001) 8902–8913, https://doi.org/10.1021/ja002179j.
[23] C. Wei, G. Han, G. Jia, J. Zhou, C. Li, Study on the interaction of porphyrin with G-quadruplex DNAs, Biophys. Chem. 137 (2008) 19–23, https://doi.org/10.1016/j.bpc.2008.06.006.
[24] F. Yang, M. Xu, X. Chen, Y. Luo, Spotlight on porphyrins: classifications, mechanisms and medical applications, Biomed. Pharmacother. 164 (2023) 114933, https://doi.org/10.1016/j.biopha.2023.114933.
[25] N. Hassanzadeh Goji, M. Ramezani, A.Sh. Saljooghi, M. Alibolandi, Porphyrin-based metal–organic frameworks: focus on diagnostic and therapeutic applications, J. Nanostructure Chem. (2022), https://doi.org/10.1007/s40097-022-00500-6.
[26] Y. Liu, P. Lei, X. Liao, C. Wang, Nanoscale metal–organic frameworks as smart nanocarriers for cancer therapy, J. Nanostruct. Chem. (2022), https://doi.org/10.1007/s40097-022-00493-2.
[27] S.N. Nangare, A.G. Patil, S.M. Chandankar, P.O. Patil, Nanostructured metal–organic framework-based luminescent sensor for chemical sensing: current challenges and future prospects, J. Nanostruct. Chem. 13 (2023) 197–242, https://doi.org/10.1007/s40097-022-00479-0.
[28] L.-N. Zhu, B. Wu, D.-M. Kong, Specific recognition and stabilization of monomeric and multimeric G-quadruplexes by cationic porphyrin TMPipEOPP under molecular crowding conditions, Nucleic Acids Res. 41 (2013) 4324–4335, https://doi.org/10.1093/nar/gkt103.
[29] N. Sabharwal, J. Chen, J. Lee, C. Gangemi, A. D'Urso, L. Yatsunyk, Interactions between spermine-derivatized tentacle porphyrins and the human telomeric DNA G-Quadruplex, Int. J. Mol. Sci. 19 (2018) 3686, https://doi.org/10.3390/ijms19113686.
[30] C.M.A. Gangemi, R. Randazzo, M.E. Fragalà, G.A. Tomaselli, F.P. Ballistreri, A. Pappalardo, R.M. Toscano, G. Trusso Sfrazzetto, R. Purrello, A. D'Urso, Hierarchically controlled protonation/aggregation of a porphyrin–spermine derivative, New J. Chem. 39 (2015) 6722–6725, https://doi.org/10.1039/C5NJ01264C.
[31] A. D'Urso, R. Randazzo, V. Rizzo, C.M.A. Gangemi, V. Romanucci, A. Zarrelli, G. Tomaselli, D. Milardi, N. Borbone, R. Purrello, G. Piccialli, G. Di Fabio, G. Oliviero, Stabilization vs. destabilization of G-quadruplex superstructures: the role of the porphyrin derivative having spermine arms, Phys. Chem. Chem. Phys. 19 (2017) 17404–17410, https://doi.org/10.1039/C7CP02816D.
[32] N. Borbone, J. Amato, G. Oliviero, V. D'Atri, V. Gabelica, E. De Pauw, G. Piccialli, L. Mayol, d(CGGTGGT) forms an octameric parallel G-quadruplex via stacking of unusual G(:C):G(:C):G(:C):G(:C) octads, Nucleic Acids Res. 39 (2011) 7848–7857, https://doi.org/10.1093/nar/gkr489.
[33] V. D'Atri, N. Borbone, J. Amato, V. Gabelica, S. D'Errico, G. Piccialli, L. Mayol, G. Oliviero, DNA-based nanostructures: the effect of the base sequence on octamer formation from d(XGGYGGT) tetramolecular G-quadruplexes, Biochimie 99 (2014) 119–128, https://doi.org/10.1016/j.biochi.2013.11.020.
[34] M. Marzano, A.P. Falanga, P. Dardano, S. D'Errico, I. Rea, M. Terracciano, L. De Stefano, G. Piccialli, N. Borbone, G. Oliviero, π-π stacked DNA G-wire nanostructures formed by a short G-rich oligonucleotide containing a 3′-3′ inversion of polarity site, Org. Chem. Front. 7 (2020) 2187–2195, https://doi.org/10.1039/D0QO00561D.
[35] G. Oliviero, S. D'Errico, B. Pinto, F. Nici, P. Dardano, I. Rea, L. De Stefano, L. Mayol, G. Piccialli, N. Borbone, Self-assembly of G-rich oligonucleotides incorporating a 3′-3′ inversion of polarity site: a new route towards G-wire DNA nanostructures, ChemistryOpen 6 (2017) 599–605, https://doi.org/10.1002/open.201700024.
[36] C. Wei, G. Jia, J. Yuan, Z. Feng, C. Li, A spectroscopic study on the interactions of porphyrin with G-quadruplex DNAs, Biochemistry 45 (2006) 6681–6691, https://doi.org/10.1021/bi052356z.
[37] X. Yao, D. Song, T. Qin, C. Yang, Z. Yu, X. Li, K. Liu, H. Su, Interaction between G-quadruplex and zinc cationic porphyrin: the role of the axial water, Sci. Rep. 7 (2017) 10951, https://doi.org/10.1038/s41598-017-11413-8.
[38] P. Zhao, J.-Z. Lu, F.-Y. Hong, B.-H. Ou, F. Zhang, L. Ma, H. Guo, Shedding light on the interactions of guanine quadruplexes with tricationic metalloporphyrins, Spectrochim. Acta A Mol. Biomol. Spectrosc. 108 (2013) 1–7, https://doi.org/10.1016/j.saa.2013.01.074.
[39] R.F. Pasternack, E.J. Gibbs, J.J. Villafranca, Interactions of porphyrins with nucleic acids, Biochemistry 22 (1983) 2406–2414, https://doi.org/10.1021/bi00279a016.
[40] C. Wei, G. Jia, J. Zhou, G. Han, C. Li, Evidence for the binding mode of porphyrins to G-quadruplex DNA, Phys. Chem. Chem. Phys. 11 (2009) 4025, https://doi.org/10.1039/b901027k.
[41] R.F. Pasternack, Circular dichroism and the interactions of water soluble porphyrins with DNA—a minireview, Chirality 15 (2003) 329–332, https://doi.org/10.1002/chir.10206.
[42] G. Pescitelli, S. Gabriel, Y. Wang, J. Fleischhauer, R.W. Woody, N. Berova, Theoretical analysis of the porphyrin−porphyrin exciton interaction in circular dichroism spectra of dimeric tetraarylporphyrins, J. Am. Chem. Soc. 125 (2003) 7613–7628, https://doi.org/10.1021/ja030047v.
[43] M.J. Morris, K.L. Wingate, J. Silwal, T.C. Leeper, S. Basu, The porphyrin TmPyP4 unfolds the extremely stable G-quadruplex in MT3-MMP mRNA and alleviates its repressive effect to enhance translation in eukaryotic cells, Nucleic Acids Res. 40 (2012) 4137–4145, https://doi.org/10.1093/nar/gkr1308.
[44] N. Ofer, P. Weisman-Shomer, J. Shklover, M. Fry, The quadruplex r(CGG)n destabilizing cationic porphyrin TMPyP4 cooperates with hnRNPs to increase the translation efficiency of fragile X premutation mRNA, Nucleic Acids Res. 37 (2009) 2712–2722, https://doi.org/10.1093/nar/gkp130.
[45] R.F. Pasternack, P.J. Collings, Resonance light scattering: a new technique for studying chromophore aggregation, Science 269 (1995) 935–939, https://doi.org/10.1126/science.7638615.
[46] R.F. Pasternack, C. Bustamante, P.J. Collings, A. Giannetto, E.J. Gibbs, Porphyrin assemblies on DNA as studied by a resonance light-scattering technique, J. Am. Chem. Soc. 115 (1993) 5393–5399, https://doi.org/10.1021/ja00066a006.
[47] R.T. Wheelhouse, D. Sun, H. Han, F.X. Han, L.H. Hurley, Cationic porphyrins as telomerase inhibitors: the interaction of tetra-(N-methyl-4-pyridyl)porphine with quadruplex DNA, J. Am. Chem. Soc. 120 (1998) 3261–3262, https://doi.org/10.1021/ja973792e.
[48] F.X. Han, R.T. Wheelhouse, L.H. Hurley, Interactions of TMPyP4 and TMPyP2 with quadruplex DNA. Structural basis for the differential effects on telomerase inhibition, J. Am. Chem. Soc. 121 (1999) 3561–3570, https://doi.org/10.1021/ja984153m.
[49] I. Lubitz, N. Borovok, A. Kotlyar, Interaction of monomolecular G4-DNA nanowires with TMPyP: evidence for intercalation, Biochemistry 46 (2007) 12925–12929, https://doi.org/10.1021/bi701301u.
[50] F. Aboul-ela, A.I.H. Murchie, D.M.J. Lilley, NMR study of parallel-stranded tetraplex formation by the hexadeoxynucleotide d(TG4T), Nature 360 (1992) 280–282, https://doi.org/10.1038/360280a0.
[51] P. Pathak, W. Yao, K.D. Hook, R. Vik, F.R. Winnerdy, J.Q. Brown, B.C. Gibb, Z. F. Pursell, A.T. Phan, J. Jayawickramarajah, Bright G-quadruplex nanostructures functionalized with porphyrin lanterns, J. Am. Chem. Soc. 141 (2019) 12582–12591, https://doi.org/10.1021/jacs.9b03250.
[52] J.T. Davis, G-quartets 40 years later: from 5′-GMP to molecular biology and supramolecular chemistry, Angew. Chem. Int. Ed. 43 (2004) 668–698, https://doi.org/10.1002/anie.200300589.
[53] J. Vesenka, T. Marsh, The diameter of duplex and quadruplex DNA measured by scanning probe microscopy, Scanning Microsc. 12 (1998) 329–342.
[54] K. Bose, C.J. Lech, B. Heddi, A.T. Phan, High-resolution AFM structure of DNA G-wires in aqueous solution, Nat. Commun. 9 (2018) 1959, https://doi.org/10.1038/s41467-018-04016-y.
[55] M.S. Searle, H.E.L. Williams, C.T. Gallagher, R.J. Grant, M.F.G. Stevens, Structure and K^+ ion-dependent stability of a parallel-stranded DNA quadruplex containing a core A-tetrad, Org. Biomol. Chem. 2 (2004) 810–812, https://doi.org/10.1039/b314559j.
[56] D. Pavc, N. Sebastian, L. Spindler, I. Drevenšek-Olenik, G.K. Podboršek, J. Plavec, P. Šket, Understanding self-assembly at molecular level enables controlled design of DNA G-wires of different properties, Nat. Commun. 13 (2022) 1062, https://doi.org/10.1038/s41467-022-28726-6.
[57] A.B. Kotlyar, N. Borovok, T. Molotsky, H. Cohen, E. Shapir, D. Porath, Long, monomolecular guanine-based nanowires, Adv. Mater. 17 (2005) 1901–1905, https://doi.org/10.1002/adma.200401997.
[58] T.C. Marsh, J. Vesenka, E. Henderson, A new DNA nanostructure, the G-wire, imaged by scanning probe microscopy, Nucleic Acids Res. 23 (1995) 696–700, https://doi.org/10.1093/nar/23.4.696.
[59] S. Kolesnikova, M. Hubálek, L. Bednárová, J. Cvačka, E.A. Curtis, Multimerization rules for G-quadruplexes, Nucleic Acids Res. 45 (2017) 8684–8696, https://doi.org/10.1093/nar/gkx637.
[60] S. Benito, A. Ferrer, S. Benabou, A. Aviñó, R. Eritja, R. Gargallo, Evaluation of the effect of polymorphism on G-quadruplex-ligand interaction by means of spectroscopic and chromatographic techniques, Spectrochim. Acta A Mol. Biomol. Spectrosc. 196 (2018) 185–195, https://doi.org/10.1016/j.saa.2018.02.006.

[61] F. Greco, M. Marzano, A.P. Falanga, M. Terracciano, G. Piccialli, G.N. Roviello, S. D'Errico, N. Borbone, G. Oliviero, Cytosine-rich oligonucleotides incorporating a non-nucleotide loop: a further step towards the obtainment of physiologically stable i-motif DNA, Int. J. Biol. Macromol. 219 (2022) 626–636, https://doi.org/10.1016/j.ijbiomac.2022.08.016.

[62] M.C. Miller, H.T. Le, W.L. Dean, P.A. Holt, J.B. Chaires, J.O. Trent, Polymorphism and resolution of oncogene promoter quadruplex-forming sequences, Org. Biomol. Chem. 9 (2011) 7633, https://doi.org/10.1039/c1ob05891f.

[63] M.Y. Kim, M. Gleason-Guzman, E. Izbicka, D. Nishioka, L.H. Hurley, The different biological effects of Telomestatin and TMPyP4 can be attributed to their selectivity for interaction with intramolecular or intermolecular G-quadruplex structures, Cancer Res. 63 (2003) 3247–3256.

[64] A. Ferdous, Poly(L-lysine)-graft-dextran copolymer: amazing effects on triplex stabilization under physiological pH and ionic conditions (in vitro), Nucleic Acids Res. 26 (1998) 3949–3954, https://doi.org/10.1093/nar/26.17.3949.

[65] N. Kumar, R. Basundra, S. Maiti, Elevated polyamines induce c-MYC overexpression by perturbing quadruplex–WC duplex equilibrium, Nucleic Acids Res. 37 (2009) 3321–3331, https://doi.org/10.1093/nar/gkp196.